APPLICATION OF THE UNSTEADY COMPRESSIBLE SOURCE AND DOUBLET PANEL METHOD TO FLUTTER CALCULATIONS

Grigorios Dimitriadis[1], Spyridon Kilimtzidis[2], Vassilis Kostopoulos[2], Vito Laraspata[3], Leonardo Soria[3]

[1]Aerospace and Mechanical Engineering Department, University of Liège, Belgium
gdimitriadis@uliege.be

[2]Department of Mechanical Engineering & Aeronautics, University of Patras, Greece
s.kilimtzidis@upnet.gr
kostopoulos@upatras.gr

[3]Department of Mathematics, Mechanics and Management, Politecnico di Bari, Italy
v.laraspata1@studenti.poliba.it
leonardo.soria@poliba.it

Keywords: Aeroelasticity, Flutter, Source and Doublet Panel Method

Abstract: The Source and Doublet Panel Method (SDPM) developed by Morino in the 1970s can model unsteady compressible ideal flow around wings and bodies. In this work, the SDPM is adapted to the calculation of aeroelastic solutions for wings. A second order nonlinear version of Bernoulli's equation is transformed to the frequency domain and written in terms of the generalized mode shapes and displacements. It is shown that the unsteady pressure component at the oscillating frequency is a linear function of the generalized displacements and can therefore be used to formulate a linear flutter problem. The proposed approach has several advantages: the exact geometry is modelled, including thickness, camber, twist and dihedral effects, the motion of the surface can be represented using all six degrees of freedom, the pressure calculation is of higher order and the generalised aerodynamic mass, damping and stiffness load terms are calculated separately. The complete procedure is validated using the experimental data from the weakened AGARD 445.6 wing and three rectangular wings with pitch and plunge degrees of freedom.

1 INTRODUCTION

This work presents an aeroelastic prediction methodology based on the subsonic unsteady Source and Doublet Panel Method (SDPM) dvelopped by Morino et al [1–3]. This method models all aspects of wing geometries, including the exact airfoil shape, twist, dihedral, winglets etc. It was recently improved by means of a nonlinear pressure calculation and the zero normal mass flux boundary condition [4, 5], so that it can now predict unsteady pressure distributions with better accuracy. Furthermore, it has been extended to the calculation of the aerodynamic stability derivatives of complete aircraft configurations [6, 7]. Here, the SDPM is extended to flutter calculations and the resulting technique is applied to standard experimental flutter test cases.

2 QUASI-FIXED MODELLING

Quasi-fixed aeroelastic modelling assumes that points on the surface of a body, $\mathbf{x}_s(t)$, can be expressed as

$$\mathbf{x}_s(t) = \mathbf{x}_{s_0} + \mathbf{x}'(\mathbf{x}_{s_0}, t)$$

where $\mathbf{x}_{s_0}$ is the initial shape and $\mathbf{x}'(\mathbf{x}_{s_0}, t)$ a small time-varying deformation with $||\mathbf{x}'|| \ll ||\mathbf{x}_{s_0}||$. The local rotation angles are denoted by $\phi(\mathbf{x}_{s_0}, t)$ for roll around the x axis, $\theta(\mathbf{x}_{s_0}, t)$ for pitch around the y axis and $\psi(\mathbf{x}_{s_0}, t)$ for yaw around the z axis. For small rotation angles, the rotation matrix can be linearised such that

$$\boldsymbol{R}(\mathbf{x}_{s_0}, t) = \begin{pmatrix} 1 & -\psi(\mathbf{x}_{s_0}, t) & -\theta(\mathbf{x}_{s_0}, t) \\ \psi(\mathbf{x}_{s_0}, t) & 1 & -\phi(\mathbf{x}_{s_0}, t) \\ \theta(\mathbf{x}_{s_0}, t) & \phi(\mathbf{x}_{s_0}, t) & 1 \end{pmatrix}$$

as long as the axis system and the positive angle directions are defined using the right-hand rule. As developed in the present work, the SDPM uses an axis system whereby the x axis is positive in the downstream direction, the y axis in the left direction when looking downstream and the z axis in the upwards direction. Consequently, in order to retain the positive directions for the pitch and yaw that are usually used in aerodynamics, the signs of ϕ and ψ must be changed, such that the rotation matrix becomes

$$\boldsymbol{R}(\mathbf{x}_{s_0}, t) = \begin{pmatrix} 1 & \psi(\mathbf{x}_{s_0}, t) & -\theta(\mathbf{x}_{s_0}, t) \\ -\psi(\mathbf{x}_{s_0}, t) & 1 & \phi(\mathbf{x}_{s_0}, t) \\ \theta(\mathbf{x}_{s_0}, t) & -\phi(\mathbf{x}_{s_0}, t) & 1 \end{pmatrix}$$

In quasi-fixed modelling, the shape of the surface remains constant in time and equal to $\mathbf{x}_{s_0}(t)$. The motion of the surface is represented by the unsteady relative velocity between the surface and the flow, $-\dot{\mathbf{x}}'_s(t)$, and by the rotation of the free stream

$$\boldsymbol{Q}_\infty(\mathbf{x}_{s_0}, t) = \boldsymbol{R}(\mathbf{x}_{s_0}, t)\boldsymbol{Q}_\infty(0) = \begin{pmatrix} 1 & \psi(\mathbf{x}_{s_0}, t) & -\theta(\mathbf{x}_{s_0}, t) \\ -\psi(\mathbf{x}_{s_0}, t) & 1 & \phi(\mathbf{x}_{s_0}, t) \\ \theta(\mathbf{x}_{s_0}, t) & -\phi(\mathbf{x}_{s_0}, t) & 1 \end{pmatrix} \boldsymbol{Q}_\infty(0) \quad (1)$$

where $\boldsymbol{Q}_\infty(0)$ is the initial free stream velocity.

Within the context of a finite element representation of the surface, $\mathbf{x}'(\mathbf{x}_{s_0}, t)$ would be the translational and $(\phi(\mathbf{x}_{s_0}, t), \theta(\mathbf{x}_{s_0}, t), \psi(\mathbf{x}_{s_0}, t))$ the rotational degrees of freedom of the node lying at $\mathbf{x}_{s_0}$. If there are N_{FE} nodes on the (x_{s_0}, y_{s_0}) plane, then the equation of motion of the structure is

$$\boldsymbol{M}\ddot{\mathbf{y}} + \boldsymbol{K}\mathbf{y} = \mathbf{0}$$

where $\boldsymbol{M}, \boldsymbol{K}$ are $6N_{\text{FE}} \times 6N_{\text{FE}}$ mass and stiffness matrices and $\mathbf{y}$ is a $6N_{\text{FE}} \times 1$ vector of nodal degrees of freedom of the form

$$\mathbf{y} = \begin{pmatrix} x'_1 & y'_1 & z'_1 & \phi_1 & \theta_1 & \psi_1 & \dots & x'_{N_{\text{FE}}} & y'_{N_{\text{FE}}} & z'_{N_{\text{FE}}} & \phi_{N_{\text{FE}}} & \theta_{N_{\text{FE}}} & \psi_{N_{\text{FE}}} \end{pmatrix}^T$$

In modal space, the equation of motion is written as

$$\boldsymbol{A}\ddot{\mathbf{q}} + \boldsymbol{E}\mathbf{q} = \mathbf{0} \quad (2)$$

where $\mathbf{y} = \boldsymbol{\Phi}\mathbf{q}$, $\boldsymbol{A} = \boldsymbol{\Phi}^T\boldsymbol{M}\boldsymbol{\Phi}$ and $\boldsymbol{E} = \boldsymbol{\Phi}^T\boldsymbol{K}\boldsymbol{\Phi}$. The $6N_{\text{FE}} \times K$ mode shape matrix, $\boldsymbol{\Phi}$, is obtained from the solution of the generalized eigenvalue problem

$$\boldsymbol{K}\boldsymbol{V} = \boldsymbol{M}\boldsymbol{V}\boldsymbol{\Lambda}$$

where $\boldsymbol{V}$ is the $6N_{\mathrm{FE}} \times 6N_{\mathrm{FE}}$ eigenvector matrix and $\boldsymbol{\Lambda}$ the $6N_{\mathrm{FE}} \times 6N_{\mathrm{FE}}$ eigenvalue matrix. Then, $\boldsymbol{\Phi}$ is the matrix formed by the first K columns of $\boldsymbol{V}$, while $\boldsymbol{A}$ and $\boldsymbol{E}$ are $K \times K$ diagonal matrices and $\boldsymbol{q}(t)$ is the $K \times 1$ generalized coordinate vector. Then, the displacements and rotations of the wing's surface can be expressed as

$$\boldsymbol{x}'(t) = \boldsymbol{\Phi}_x \boldsymbol{q}(t), \ \boldsymbol{y}'(t) = \boldsymbol{\Phi}_y \boldsymbol{q}(t), \ \boldsymbol{z}'(t) = \boldsymbol{\Phi}_z \boldsymbol{q}(t),$$

$$\boldsymbol{\phi}(t) = \boldsymbol{\Phi}_\phi \boldsymbol{q}(t), \ \boldsymbol{\theta}(t) = \boldsymbol{\Phi}_\theta \boldsymbol{q}(t), \ \boldsymbol{\psi}(t) = \boldsymbol{\Phi}_\psi \boldsymbol{q}(t)$$

Finally, if $\boldsymbol{Q}_\infty(0) = (U_\infty, \ V_\infty, \ W_\infty)$, equation 1 becomes

$$
\begin{aligned}
\boldsymbol{U}_\infty(t) &= U_\infty + V_\infty \boldsymbol{\Phi}_\psi \boldsymbol{q}(t) - W_\infty \boldsymbol{\Phi}_\theta \boldsymbol{q}(t) \\
\boldsymbol{V}_\infty(t) &= -U_\infty \boldsymbol{\Phi}_\psi \boldsymbol{q}(t) + V_\infty + W_\infty \boldsymbol{\Phi}_\phi \boldsymbol{q}(t) \\
\boldsymbol{W}_\infty(t) &= U_\infty \boldsymbol{\Phi}_\theta \boldsymbol{q}(t) - V_\infty \boldsymbol{\Phi}_\phi \boldsymbol{q}(t) + W_\infty
\end{aligned}
$$

Adding the unsteady relative velocity term, $-\dot{\mathbf{x}}'_s(t)$, written out for each of the nodes, the total relative flow velocity due to the flexible motion becomes

$$
\begin{aligned}
\boldsymbol{u}_{\mathrm{rel}}(t) &= U_\infty + V_\infty \boldsymbol{\Phi}_\psi \boldsymbol{q}(t) - W_\infty \boldsymbol{\Phi}_\theta \boldsymbol{q}(t) - \boldsymbol{\Phi}_x \dot{\boldsymbol{q}}(t) \\
\boldsymbol{v}_{\mathrm{rel}}(t) &= -U_\infty \boldsymbol{\Phi}_\psi \boldsymbol{q}(t) + V_\infty + W_\infty \boldsymbol{\Phi}_\phi \boldsymbol{q}(t) - \boldsymbol{\Phi}_y \dot{\boldsymbol{q}}(t) \\
\boldsymbol{w}_{\mathrm{rel}}(t) &= U_\infty \boldsymbol{\Phi}_\theta \boldsymbol{q}(t) - V_\infty \boldsymbol{\Phi}_\phi \boldsymbol{q}(t) + W_\infty - \boldsymbol{\Phi}_z \dot{\boldsymbol{q}}(t)
\end{aligned}
\tag{3}
$$

Note that, if the wing or aircraft is flying with mean airspeed Q_∞ at a mean angle of attack α_0 and mean sideslip angle β_0, then [8]

$$U_\infty = Q_\infty \cos \alpha_0 \cos \beta_0, \ V_\infty = -Q_\infty \sin \beta_0, \ W_\infty = Q_\infty \sin \alpha_0 \cos \beta_0 \tag{4}$$

3 AEROELASTIC SOURCE AND DOUBLET PANEL METHOD

The fundamental equation of the unsteady compressible Source and Doublet Panel Method (SDPM) is Green's theorem in the frequency domain [1, 9]

$$\left(\bar{\boldsymbol{B}}_\phi(\omega) - \frac{1}{2} \boldsymbol{I} \right) \boldsymbol{\mu}(\omega) + \bar{\boldsymbol{C}}_\phi(\omega) \boldsymbol{\mu}_w(\omega) = -\bar{\boldsymbol{A}}_\phi(\omega) \boldsymbol{\sigma}(\omega) \tag{5}$$

Equation 5 is written out for the N panels on the surface of a wing and the N_w panels on the flat wake, such that ω is the frequency in rad/s, $\bar{\boldsymbol{A}}_\phi(\omega)$, $\bar{\boldsymbol{B}}_\phi(\omega)$ are $N \times N$ source and doublet influence coefficient matrices, $\bar{\boldsymbol{C}}_\phi(\omega)$ is the $N \times N_w$ doublet influence coefficient matrix of the wake on the wing, $\boldsymbol{\sigma}(\omega)$, $\boldsymbol{\mu}(\omega)$ are $N \times 1$ vectors of the source and doublet strengths on the wing panels and $\boldsymbol{\mu}_w(\omega)$ is the $N_w \times 1$ vector of the doublet strengths on the wake panels.

The source strength vector $\boldsymbol{\sigma}(\omega)$ is calculated from the zero mass flux normal to the surface boundary condition [4, 5], such that

$$\boldsymbol{\sigma}(\omega) = \mathrm{i}\Omega M_\infty \boldsymbol{n}_\xi \circ \boldsymbol{\mu}(\omega) - \left(\frac{1}{\beta} \boldsymbol{u}_m(\omega) \circ \boldsymbol{n}_\xi + \boldsymbol{v}_m(\omega) \circ \boldsymbol{n}_\eta + \boldsymbol{w}_m(\omega) \circ \boldsymbol{n}_\zeta \right) \tag{6}$$

where M_∞ is the free stream Mach number, $\Omega = \omega/a_\infty\beta$, a_∞ is the free stream speed of sound, $\beta = \sqrt{1 - M_\infty^2}$ is the subsonic compressibility factor, $\boldsymbol{n}_\xi$, $\boldsymbol{n}_\eta$, $\boldsymbol{n}_\zeta$ are $N \times 1$ vectors of the three components of unit vectors normal to the panels and pointing into the flow, $\xi = x/\beta$, $\eta = y$, $\zeta = z$ are Prandtl-Glauert coordinates and the operator $\circ$ is used to denote the Hadamard

product, i.e. element-by-element multiplication of vectors of the same size. Finally, $\boldsymbol{u}_m(\omega)$, $\boldsymbol{v}_m(\omega)$, $\boldsymbol{w}_m(\omega)$ are obtained from the Fourier Transform of equations 3, after interpolating the mode shapes of the finite element model onto the control points of the SDPM panels, that is

$$
\begin{array}{rcl}
\boldsymbol{u}_m(\omega) & = & U_\infty \delta(\omega) + V_\infty \tilde{\boldsymbol{\Phi}}_\psi \boldsymbol{q}(\omega) - W_\infty \tilde{\boldsymbol{\Phi}}_\theta \boldsymbol{q}(\omega) - \mathrm{i}\omega \tilde{\boldsymbol{\Phi}}_x \boldsymbol{q}(\omega) \\
\boldsymbol{v}_m(\omega) & = & -U_\infty \tilde{\boldsymbol{\Phi}}_\psi \boldsymbol{q}(\omega) + V_\infty \delta(\omega) + W_\infty \tilde{\boldsymbol{\Phi}}_\phi \boldsymbol{q}(\omega) - \mathrm{i}\omega \tilde{\boldsymbol{\Phi}}_y \boldsymbol{q}(\omega) \\
\boldsymbol{w}_m(\omega) & = & U_\infty \tilde{\boldsymbol{\Phi}}_\theta \boldsymbol{q}(\omega) - V_\infty \tilde{\boldsymbol{\Phi}}_\phi \boldsymbol{q}(\omega) + W_\infty \delta(\omega) - \mathrm{i}\omega \tilde{\boldsymbol{\Phi}}_z \boldsymbol{q}(\omega)
\end{array}
\tag{7}
$$

where the tilde denotes interpolated quantities and $\delta(\omega)$ is the Kronecker delta function.

Equation 5 constitutes a set of N equations with $N + N_w$ unknowns, the doublet strength vectors $\boldsymbol{\mu}(\omega)$ and $\boldsymbol{\mu}_w(\omega)$. Imposing the Kutta condition and assuming that the wake vorticity travels at the free stream velocity, the doublet strengths in the wake can be written in terms of the doublet strengths of the trailing edge panels on the upper and lower surfaces. Then, equation 5 becomes

$$
\left(\bar{\boldsymbol{B}}_\phi(\omega) - \frac{1}{2}\boldsymbol{I} + \bar{\boldsymbol{C}}_\phi(\omega)\boldsymbol{P}_e(\omega)\boldsymbol{P}_c \right) \boldsymbol{\mu}(\omega) = -\bar{\boldsymbol{A}}_\phi(\omega)\boldsymbol{\sigma}(\omega)
\tag{8}
$$

where $\boldsymbol{P}_c$ and $\boldsymbol{P}_e(\omega)$ are given by

$$
\boldsymbol{P}_c = \begin{pmatrix} \boldsymbol{0}_{n\times(2m-1)n} & \boldsymbol{I}_n \end{pmatrix} - \begin{pmatrix} \boldsymbol{I}_n & \boldsymbol{0}_{n\times(2m-1)n} \end{pmatrix}
\tag{9}
$$

$$
\boldsymbol{P}_e(\omega) = \begin{pmatrix} \boldsymbol{I}_n \mathrm{e}^{-\mathrm{i}\omega c_0/mU_\infty} \\ \boldsymbol{I}_n \mathrm{e}^{-\mathrm{i}\omega 2c_0/mU_\infty} \\ \vdots \\ \boldsymbol{I}_n \mathrm{e}^{-\mathrm{i}\omega m_w c_0/mU_\infty} \end{pmatrix} = \begin{pmatrix} \boldsymbol{I}_n \mathrm{e}^{-\mathrm{i}\omega 2k/m} \\ \boldsymbol{I}_n \mathrm{e}^{-\mathrm{i}\omega 4k/m} \\ \vdots \\ \boldsymbol{I}_n \mathrm{e}^{-\mathrm{i}\omega 2m_w k/m} \end{pmatrix}
\tag{10}
$$

m_w is the number of wake panels in the streamwise direction, m is the number of upper surface wing panels in the chordwise direction, n is the number of wing panels in the spanwise direction, the total number of wing panels is $N = 2mn$, c_0 is the root chord of the wing and

$$
k = \frac{\omega c_0}{2U_\infty}
$$

is the reduced frequency. The elements of matrices $\bar{\boldsymbol{A}}(\omega)$, $\bar{\boldsymbol{B}}_\phi(\omega)$ and $\bar{\boldsymbol{C}}_\phi(\omega)$ are given by [4]

$$
\begin{array}{rcl}
\bar{A}_{\phi_{IJ}}(\omega) & = & \mathrm{e}^{-\mathrm{i}\Omega(-M_\infty(\xi_{c_I}-\xi_{c_J})+r(\boldsymbol{\xi}_{c_I},\boldsymbol{\xi}_{c_J}))} A_{\phi_{I,J}}
\end{array}
\tag{11}
$$

$$
\begin{array}{rcl}
\bar{B}_{\phi_{IJ}}(\omega) & = & -\mathrm{i}\Omega \mathrm{e}^{-\mathrm{i}\Omega(-M_\infty(\xi_{c_I}-\xi_{c_J})+r(\boldsymbol{\xi}_{c_I},\boldsymbol{\xi}_{c_J}))} M_\infty n_\xi(\boldsymbol{\xi}_{c_J}) A_{\phi_{I,J}} \\
& & + (1 + \mathrm{i}\Omega r(\boldsymbol{\xi}_{c_I},\boldsymbol{\xi}_{c_J})) \mathrm{e}^{-\mathrm{i}\Omega(-M_\infty(\xi_{c_I}-\xi_{c_J})+r(\boldsymbol{\xi}_{c_I},\boldsymbol{\xi}_{c_J}))} B_{\phi_{I,J}}
\end{array}
\tag{12}
$$

for $I = 1,\ldots,N$, $J = 1,\ldots,N$ and

$$
\bar{C}_{\phi_{IJ}}(\omega) = (1 + \mathrm{i}\Omega r(\boldsymbol{\xi}_{c_I},\boldsymbol{\xi}_{c_J})) \mathrm{e}^{-\mathrm{i}\Omega(-M_\infty(\xi_{c_I}-\xi_{c_J})+r(\boldsymbol{\xi}_{c_I},\boldsymbol{\xi}_{c_J}))} C_{\phi_{I,J}}
\tag{13}
$$

for $I = 1,\ldots,N$, $J = 1,\ldots,N_w$. In these last three expressions, $\boldsymbol{\xi}_{c_{I,J}} = (\xi_{c_{I,J}}, \eta_{c_{I,J}}, \zeta_{c_{I,J}})$ are the Prandtl-Glauert coordinates of the Ith or Jth panel control points while the $N \times N$ matrices $\boldsymbol{A}_\phi$, $\boldsymbol{B}_\phi$ and $\boldsymbol{C}_\phi$ are the source and doublet influence coefficient matrices obtained for steady potential flow using the approach by Hess and Smith [10]. Furthermore, it has been assumed that the wake is flat and aligned with the x axis, so that $n_\xi(\boldsymbol{\xi}_{c_J}) = 0$ for all the wake panels. Also note that the compressible frequency Ω can be written as

$$
\Omega = \frac{2kM_\infty}{c_0\beta}
$$

4

so that $\bar{A}_{\phi_{IJ}}(k, M_\infty)$, $\bar{B}_{\phi_{IJ}}(k, M_\infty)$ and $\bar{C}_{\phi_{IJ}}(k, M_\infty)$ are functions only of the wing's geometry, the panel grid, the Mach number and the reduced frequency.

Equations 6 to 8 now form a set of N equations with N unknowns, the wing doublet strengths $\boldsymbol{\mu}(\omega)$. The solution can be written as

$$\boldsymbol{\mu}(k) = -\boldsymbol{K}(k)\boldsymbol{\mu}_n(k) \tag{14}$$

where

$$\boldsymbol{K}(k) = \left(\frac{2\mathrm{i}kM_\infty^2}{c_0\beta} \bar{\boldsymbol{A}}_\phi(k) \circ \boldsymbol{n}_\xi + \bar{\boldsymbol{B}}_\phi(k) - \frac{1}{2}\boldsymbol{I} + \bar{\boldsymbol{C}}_\phi(k)\boldsymbol{P}_e(k)\boldsymbol{P}_c \right)^{-1} \bar{\boldsymbol{A}}_\phi(k)$$

$$\boldsymbol{\mu}_n(k) = -\left(\frac{1}{\beta}\boldsymbol{u}_m(k) \circ \boldsymbol{n}_\xi + \boldsymbol{v}_m(k) \circ \boldsymbol{n}_\eta + \boldsymbol{w}_m(k) \circ \boldsymbol{n}_\zeta \right)$$

and the Hadamard operator is also used to denote the element-by-element multiplication of each of the columns of a matrix by the same column vector. In most subsonic aircraft aeroelastic applications $k \leq 2$ and $\boldsymbol{n}_\xi$ is small except around the leading edge, so that the first term in the expression for $\boldsymbol{K}(k)$ can be neglected.

3.1 Calculation of the surface flow velocities

The next step is to calculate the perturbation flow velocities ϕ_x, ϕ_y and ϕ_z on the surface. This calculation can be carried out in Prandtl-Glauert coordinates, recalling that the doublet strength on the surface is the potential, $\mu(\boldsymbol{\xi}_{c_I}, k) = \phi(\boldsymbol{\xi}_{c_I}, k)$. The doublet strength is differentiated numerically in the chordwise and spanwise directions and the three components of the velocity in the ξ, η, ζ directions are obtained from [4, 5]

$$
\begin{aligned}
\boldsymbol{\tau}_m(\boldsymbol{\xi}_{c_I}) \cdot (\phi_\xi(\boldsymbol{\xi}_{c_I}, k),\ \phi_\eta(\boldsymbol{\xi}_{c_I}, k),\ \phi_\zeta(\boldsymbol{\xi}_{c_I}, k)) &= \boldsymbol{\tau}_m(\boldsymbol{\xi}_{c_I}) \cdot \nabla\mu(\boldsymbol{\xi}_{c_I}, k) \\
\boldsymbol{\tau}_n(\boldsymbol{\xi}_{c_I}) \cdot (\phi_\xi(\boldsymbol{\xi}_{c_I}, k),\ \phi_\eta(\boldsymbol{\xi}_{c_I}, k),\ \phi_\zeta(\boldsymbol{\xi}_{c_I}, k)) &= \boldsymbol{\tau}_n(\boldsymbol{\xi}_{c_I}) \cdot \nabla\mu(\boldsymbol{\xi}_{c_I}, k) \\
\mathbf{n}(\boldsymbol{\xi}_{c_I}) \cdot (\phi_\xi(\boldsymbol{\xi}_{c_I}, k),\ \phi_\eta(\boldsymbol{\xi}_{c_I}, k),\ \phi_\zeta(\boldsymbol{\xi}_{c_I}, k)) &= \boldsymbol{n}(\boldsymbol{\xi}_{c_I}) \cdot \nabla\mu(\boldsymbol{\xi}_{c_I}, k)
\end{aligned}
\tag{15}
$$

where $\boldsymbol{\tau}_m(\boldsymbol{\xi}_{c_I})$, $\boldsymbol{\tau}_n(\boldsymbol{\xi}_{c_I})$ are unit vectors tangent to the surface at the control point of the Ith transformed panel and pointing in the chordwise and spanwise directions, $\boldsymbol{\tau}_m(\boldsymbol{\xi}_{c_I}) \cdot \nabla\mu(\boldsymbol{\xi}_{c_I}, k)$, $\boldsymbol{\tau}_n(\boldsymbol{\xi}_{c_I}) \cdot \nabla\mu(\boldsymbol{\xi}_{c_I}, k)$ are the derivatives of the doublet strength in the chordwise and spanwise directions at the Ith control point and $\boldsymbol{n}(\boldsymbol{\xi}_{c_I}) \cdot \nabla\mu(\boldsymbol{\xi}_{c_I}, k) = \sigma(\boldsymbol{\xi}_{c_I}, k)$ is the source strength on the Ith panel. Then, the surface perturbation velocities are transformed back to the original coordinates using

$$\phi_x(\mathbf{x}_{c_I}, k) = \frac{1}{\beta}\phi_\xi(\boldsymbol{\xi}_{c_I}, k),\ \ \phi_y(\mathbf{x}_{c_I}, k) = \phi_\eta(\boldsymbol{\xi}_{c_I}, k),\ \ \phi_z(\mathbf{x}_{c_I}, k) = \phi_\zeta(\boldsymbol{\xi}_{c_I}, k)$$

The derivatives $\boldsymbol{\tau}_m(\boldsymbol{\xi}_{c_I}) \cdot \nabla\mu(\boldsymbol{\xi}_{c_I}, k)$, $\boldsymbol{\tau}_n(\boldsymbol{\xi}_{c_I}) \cdot \nabla\mu(\boldsymbol{\xi}_{c_I}, k)$ can be calculated using central differences, except at the leading edge, trailing edge and wingtips where forward/backward differences are used as necessary [7]. Then, the perturbation velocities in cartesian space are obtained from

$$\boldsymbol{\phi}_x(k) = \boldsymbol{K}_x(k)\boldsymbol{\mu_n}(k),\ \ \boldsymbol{\phi}_y(k) = \boldsymbol{K}_y(k)\boldsymbol{\mu_n}(k),\ \ \boldsymbol{\phi}_z(k) = \boldsymbol{K}_z(k)\boldsymbol{\mu_n}(k) \tag{16}$$

where $\boldsymbol{\phi}_x$, $\boldsymbol{\phi}_y$, $\boldsymbol{\phi}_z$ are $N \times 1$ vectors whose elements are the three components of the perturbation velocity on the control points, $\boldsymbol{K}(k)$ is given just after equation 14 and $\boldsymbol{K}_x(k)$, $\boldsymbol{K}_y(k)$, $\boldsymbol{K}_z(k)$ are $N \times N$ matrices that are functions of $\boldsymbol{K}(k)$ and the finite difference scheme.

3.2 Calculation of the aerodynamic loads

The final step is to calculate the pressure coefficient on the panels from the second order unsteady compressible Bernoulli equation [8]

$$c_p(t) = 1 - \frac{Q(t)^2}{Q_\infty^2} + \frac{M_\infty^2}{Q_\infty^2}\phi_x^2 - \frac{2}{Q_\infty^2}\phi_t + \frac{M_\infty^2}{Q_\infty^4}\phi_t^2 + \frac{2M_\infty^2}{Q_\infty^3}\phi_x\phi_t \tag{17}$$

Applying the Fourier transform leads to

$$
\begin{aligned}
c_p(\omega) = {} & \delta(\omega) - \frac{Q(\omega) * Q(\omega)}{Q_\infty^2} + \frac{M_\infty^2}{Q_\infty^2}\phi_x(\omega) * \phi_x(\omega) - \frac{2\mathrm{i}\omega}{Q_\infty^2}\phi(\omega) \\
& + \frac{M_\infty^2}{Q_\infty^4}(\mathrm{i}\omega\phi(\omega)) * (\mathrm{i}\omega\phi(\omega)) + \frac{2M_\infty^2}{Q_\infty^3}\phi_x(\omega) * (\mathrm{i}\omega\phi(\omega))
\end{aligned}
\tag{18}
$$

where the $*$ operator denotes convolution. Assuming sinusoidal motion at frequency ω_0, $\phi_x(\omega)$, $u(\omega)$, $v(\omega)$ etc have frequency components at $-\omega_0$, 0 and ω_0 and can be written as vectors with three elements, that is

$$
\begin{aligned}
\phi_x(\omega) &= (\phi_x^*(\omega_0),\ \phi_x(0),\ \phi_x(\omega_0)) \\
\mathrm{i}\omega\phi(\omega) &= ((\mathrm{i}\omega_0\mu(\omega_0))^*,\ 0,\ \mathrm{i}\omega_0\mu(\omega_0)) \\
u(\omega) &= (\phi_x^*(\omega_0) + u_m^*(\omega_0),\ U_\infty + \phi_x(0),\ \phi_x(\omega_0) + u_m(\omega_0)) \\
v(\omega) &= (\phi_y^*(\omega_0) + v_m^*(\omega_0),\ V_\infty + \phi_y(0),\ \phi_y(\omega_0) + v_m(\omega_0)) \\
w(\omega) &= (\phi_z^*(\omega_0) + w_m^*(\omega_0),\ W_\infty + \phi_z(0),\ \phi_z(\omega_0) + w_m(\omega_0)) \\
Q(\omega) * Q(\omega) &= u(\omega) * u(\omega) + v(\omega) * v(\omega) + w(\omega) * w(\omega)
\end{aligned}
\tag{19}
$$

where the $*$ superscript denotes the complex conjugate. Since $\phi_x(\omega)$, $\mathrm{i}\omega\phi(\omega)$, $u(\omega)$, $v(\omega)$, $w(\omega)$ all have three frequency components, $c_p(\omega)$ will have five components due to the convolution. Consequently, the third component gives $c_p(0)$, the fourth $c_p(\omega_0)$ and the fifth $c_p(2\omega_0)$. Working through the convolutions, the zero frequency component of the pressure becomes [7]

$$
\begin{aligned}
\boldsymbol{c}_p(0) = {} & 1 - \frac{2\boldsymbol{u}^*(\omega_0) \circ \boldsymbol{u}(\omega_0) + \boldsymbol{u}(0) \circ \boldsymbol{u}(0)}{Q_\infty^2} - \frac{2\boldsymbol{v}^*(\omega_0) \circ \boldsymbol{v}(\omega_0) + \boldsymbol{v}(0) \circ \boldsymbol{v}(0)}{Q_\infty^2} \\
& - \frac{2\boldsymbol{w}^*(\omega_0) \circ \boldsymbol{w}(\omega_0) + \boldsymbol{w}(0) \circ \boldsymbol{w}(0)}{Q_\infty^2} + \frac{M_\infty^2}{Q_\infty^2}\left(2\boldsymbol{\phi}_x^*(\omega_0) \circ \boldsymbol{\phi}_x(\omega_0) + \boldsymbol{\phi}_x(0) \circ \boldsymbol{\phi}_x(0)\right) \\
& + \frac{2\omega_0^2 M_\infty^2}{Q_\infty^4}\boldsymbol{\mu}^*(\omega_0) \circ \boldsymbol{\mu}(\omega_0) + \frac{2\mathrm{i}\omega_0 M_\infty^2}{Q_\infty^3}\left(\boldsymbol{\phi}_x^*(\omega_0) \circ \boldsymbol{\mu}(\omega_0) - \boldsymbol{\phi}_x(\omega_0) \circ \boldsymbol{\mu}^*(\omega_0)\right)
\end{aligned}
\tag{20}
$$

noting that $\boldsymbol{c}_p(0)$ is a $N \times K$ real matrix of the mean pressure coefficient on the control points due to each mode. The mean pressure coefficient is different to the steady value of the pressure coefficient in the absence of motion, given by

$$
\boldsymbol{c}_{p_0} = 1 - \frac{\boldsymbol{u}(0) \circ \boldsymbol{u}(0) + \boldsymbol{v}(0) \circ \boldsymbol{v}(0) + \boldsymbol{w}(0) \circ \boldsymbol{w}(0)}{Q_\infty^2} + \frac{M_\infty^2}{Q_\infty^2}\left(\boldsymbol{\phi}_x(0) \circ \boldsymbol{\phi}_x(0)\right)
\tag{21}
$$

where $\boldsymbol{c}_{p_0}$ is a $N \times 1$ vector of the steady pressure coefficient values on the control points due to the free stream only.

The pressure coefficient component at the oscillation frequency ω_0 is given by [7]

$$
\begin{aligned}
\boldsymbol{c}_p(\omega_0) = {} & -2\frac{\boldsymbol{u}(0) \circ \boldsymbol{u}(\omega_0) + \boldsymbol{v}(0) \circ \boldsymbol{v}(\omega_0) + \boldsymbol{w}(0) \circ \boldsymbol{w}(\omega_0)}{Q_\infty^2} + \frac{2M_\infty^2}{Q_\infty^2}\boldsymbol{\phi}_x(0) \circ \boldsymbol{\phi}_x(\omega_0) \\
& - \frac{2\mathrm{i}\omega_0}{Q_\infty^2}\boldsymbol{\mu}(\omega_0) + \frac{2\mathrm{i}\omega_0 M_\infty^2}{Q_\infty^3}\boldsymbol{\phi}_x(0) \circ \boldsymbol{\mu}(\omega_0)
\end{aligned}
\tag{22}
$$

so that $\boldsymbol{c}_p(\omega_0)$ is a $N \times K$ complex matrix of the oscillatory pressure component at ω_0 on the control points. The component $\boldsymbol{c}_p(2\omega_0)$ can be calculated in similar fashion, that is [7]

$$
\begin{aligned}
\boldsymbol{c}_p(2\omega_0) &= -\frac{\boldsymbol{u}(\omega_0) \circ \boldsymbol{u}(\omega_0) + \boldsymbol{v}(\omega_0) \circ \boldsymbol{v}(\omega_0) + \boldsymbol{w}(\omega_0) \circ \boldsymbol{w}(\omega_0)}{Q_\infty^2} \\
&+ \frac{M_\infty^2}{Q_\infty^2} \boldsymbol{\phi}_x(\omega_0) \circ \boldsymbol{\phi}_x(\omega_0) - \frac{\omega_0^2 M_\infty^2}{Q_\infty^4} \boldsymbol{\mu}(\omega_0) \circ \boldsymbol{\mu}(\omega_0) \\
&+ \frac{2\mathrm{i}\omega_0 M_\infty^2}{Q_\infty^3} \boldsymbol{\phi}_x(\omega_0) \circ \boldsymbol{\mu}(\omega_0)
\end{aligned}
$$

Note that the expressions for $\boldsymbol{c}_p(0)$ and $\boldsymbol{c}_p(2\omega_0)$ contain nonlinear terms in $\boldsymbol{\phi}_x(\omega_0)$, $\boldsymbol{u}(\omega_0)$, $\boldsymbol{v}(\omega_0)$, $\boldsymbol{w}(\omega_0)$, $\boldsymbol{\mu}(\omega_0)$ while the expression for $\boldsymbol{c}_p(\omega_0)$ does not. As the objective of the present work is to formulate a linear aeroelastic problem, only $\boldsymbol{c}_p(\omega_0)$ will be considered.

Substituting from equations 14 and 19 into expression 22, the pressure component at $\omega = \omega_0$ on all the panel control points becomes [7]

$$
\begin{aligned}
\boldsymbol{c}_p(\omega_0) &= -\frac{1}{\beta}(\boldsymbol{C}_0 \circ \boldsymbol{n}_\xi)\boldsymbol{u}_m - \frac{2}{Q_\infty^2}\boldsymbol{u}(0) \circ \boldsymbol{u}_m - (\boldsymbol{C}_0 \circ \boldsymbol{n}_\eta)\boldsymbol{v}_m - \frac{2}{Q_\infty^2}\boldsymbol{v}(0) \circ \boldsymbol{v}_m \\
&- (\boldsymbol{C}_0 \circ \boldsymbol{n}_\zeta)\boldsymbol{w}_m - \frac{2}{Q_\infty^2}\boldsymbol{w}(0) \circ \boldsymbol{w}_m + \frac{\mathrm{i}\omega_0}{\beta}(\boldsymbol{C}_1 \circ \boldsymbol{n}_\xi)\boldsymbol{u}_m \\
&+ \mathrm{i}\omega_0(\boldsymbol{C}_1 \circ \boldsymbol{n}_\eta)\boldsymbol{v}_m + \mathrm{i}\omega_0(\boldsymbol{C}_1 \circ \boldsymbol{n}_\zeta)\boldsymbol{w}_m
\end{aligned}
\tag{23}
$$

where

$$
\begin{aligned}
\boldsymbol{C}_0(\omega_0) &= \frac{2M_\infty^2}{Q_\infty^2}\boldsymbol{K}_x(\omega_0) \circ \boldsymbol{\phi}_x(0) - \frac{2}{Q_\infty^2}\boldsymbol{K}_x(\omega_0) \circ \boldsymbol{u}(0) - \frac{2}{Q_\infty^2}\boldsymbol{K}_y(\omega_0) \circ \boldsymbol{v}(0) \\
&- \frac{2}{Q_\infty^2}\boldsymbol{K}_z(\omega_0) \circ \boldsymbol{w}(0) \\
\boldsymbol{C}_1(\omega_0) &= \frac{2}{Q_\infty^2}\boldsymbol{K}(\omega_0) - \frac{2M_\infty^2}{Q_\infty^3}\boldsymbol{K}(\omega_0) \circ \boldsymbol{\phi}_x(0) \\
\boldsymbol{\mu}_n(0) &= -\left(\frac{U_\infty}{\beta}\boldsymbol{n}_\xi + V_\infty\boldsymbol{n}_\eta + W_\infty\boldsymbol{n}_\zeta\right)
\end{aligned}
\tag{24}
$$

and $\boldsymbol{\phi}_x(0) = \boldsymbol{K}_x(0)\boldsymbol{\mu}_n(0)$, $\boldsymbol{\phi}_y(0) = \boldsymbol{K}_y(0)\boldsymbol{\mu}_n(0)$, $\boldsymbol{\phi}_z(0) = \boldsymbol{K}_z(0)\boldsymbol{\mu}_n(0)$, $\boldsymbol{u}(0) = U_\infty + \boldsymbol{\phi}_x(0)$, $\boldsymbol{v}(0) = V_\infty + \boldsymbol{\phi}_y(0)$, $\boldsymbol{w}(0) = W_\infty + \boldsymbol{\phi}_z(0)$. It can be seen that, despite the fact that equation 17 is nonlinear, the pressure component at ω_0 in equation 23 is a linear combination of the relative velocities $\boldsymbol{u}_m$, $\boldsymbol{v}_m$, $\boldsymbol{w}_m$. Up to this point, the latter have not been specified.

For flexible motion described in modal coordinates, the relative velocities between the flow and the body are given by equation 7, such that for $\omega = \omega_0$,

$$
\begin{aligned}
\boldsymbol{u}_m(\omega_0) &= V_\infty\tilde{\boldsymbol{\Phi}}_\psi\boldsymbol{q}(\omega_0) - W_\infty\tilde{\boldsymbol{\Phi}}_\theta\boldsymbol{q}(\omega_0) - \mathrm{i}\omega_0\tilde{\boldsymbol{\Phi}}_x\boldsymbol{q}(\omega_0) \\
\boldsymbol{v}_m(\omega_0) &= -U_\infty\tilde{\boldsymbol{\Phi}}_\psi\boldsymbol{q}(\omega_0) + W_\infty\tilde{\boldsymbol{\Phi}}_\phi\boldsymbol{q}(\omega_0) - \mathrm{i}\omega_0\tilde{\boldsymbol{\Phi}}_y\boldsymbol{q}(\omega_0) \\
\boldsymbol{w}_m(\omega_0) &= U_\infty\tilde{\boldsymbol{\Phi}}_\theta\boldsymbol{q}(\omega_0) - V_\infty\tilde{\boldsymbol{\Phi}}_\phi\boldsymbol{q}(\omega_0) - \mathrm{i}\omega_0\tilde{\boldsymbol{\Phi}}_z\boldsymbol{q}(\omega_0)
\end{aligned}
\tag{25}
$$

where matrices $\boldsymbol{u}_m(\omega_0)$, $\boldsymbol{v}_m(\omega_0)$, $\boldsymbol{w}_m(\omega_0)$ have dimensions $N \times K$, so that there is one column

for each of the modes. Substituting the components of the free stream from equation 4 leads to

$$
\begin{array}{rcl}
\bar{\boldsymbol{u}}_m(k_0) & = & \bar{V}_\infty \tilde{\boldsymbol{\Phi}}_\psi \boldsymbol{q}(k_0) - \bar{W}_\infty \tilde{\boldsymbol{\Phi}}_\theta \boldsymbol{q}(k_0) - \dfrac{2\mathrm{i}k_0}{c_0} \tilde{\boldsymbol{\Phi}}_x \boldsymbol{q}(k_0) \\[2mm]
\bar{\boldsymbol{v}}_m(k_0) & = & -\bar{U}_\infty \tilde{\boldsymbol{\Phi}}_\psi \boldsymbol{q}(k_0) + \bar{W}_\infty \tilde{\boldsymbol{\Phi}}_\phi \boldsymbol{q}(k_0) - \dfrac{2\mathrm{i}k_0}{c_0} \tilde{\boldsymbol{\Phi}}_y \boldsymbol{q}(k_0) \\[2mm]
\bar{\boldsymbol{w}}_m(k_0) & = & \bar{U}_\infty \tilde{\boldsymbol{\Phi}}_\theta \boldsymbol{q}(k_0) - \bar{V}_\infty \tilde{\boldsymbol{\Phi}}_\phi \boldsymbol{q}(k_0) - \dfrac{2\mathrm{i}k_0}{c_0} \tilde{\boldsymbol{\Phi}}_z \boldsymbol{q}(k_0)
\end{array}
\tag{26}
$$

where $\bar{\boldsymbol{u}}_m(k_0) = \boldsymbol{u}_m(k_0)/Q_\infty$, $\bar{\boldsymbol{v}}_m(k_0) = \boldsymbol{v}_m(k_0)/Q_\infty$, $\bar{\boldsymbol{w}}_m(k_0) = \boldsymbol{w}_m(k_0)/Q_\infty$, $\bar{U}_\infty = U_\infty/Q_\infty$, $\bar{V}_\infty = V_\infty/Q_\infty$, $\bar{W}_\infty = W_\infty/Q_\infty$. The unsteady solution becomes

$$
\begin{array}{rcl}
\bar{\boldsymbol{\mu}}(k_0) & = & \boldsymbol{K}(k_0)\bar{\boldsymbol{\mu}}_n(k_0) \\[1mm]
\bar{\boldsymbol{\phi}}_x(k_0) & = & \boldsymbol{K}_x(k_0)\bar{\boldsymbol{\mu}}_n(k_0), \ \ \bar{\boldsymbol{\phi}}_y(k_0) = \boldsymbol{K}_y(k_0)\bar{\boldsymbol{\mu}}_n(k_0), \ \ \bar{\boldsymbol{\phi}}_z(k_0) = \boldsymbol{K}_z(k_0)\bar{\boldsymbol{\mu}}_n(k_0) \\[1mm]
\bar{\boldsymbol{\mu}}_n(k_0) & = & -\left(\dfrac{1}{\beta}\bar{\boldsymbol{u}}_m(k_0) \circ \boldsymbol{n}_\xi + \bar{\boldsymbol{v}}_m(k_0) \circ \boldsymbol{n}_\eta + \bar{\boldsymbol{w}}_m(k_0) \circ \boldsymbol{n}_\zeta \right)
\end{array}
\tag{27}
$$

where $\bar{\boldsymbol{\phi}}_x(k_0) = \boldsymbol{\phi}_x(k_0)/Q_\infty$, $\bar{\boldsymbol{\phi}}_x(k_0) = \boldsymbol{\phi}_x(k_0)/Q_\infty$, $\bar{\boldsymbol{\phi}}_y(k_0) = \boldsymbol{\phi}_y(k_0)/Q_\infty$, $\bar{\boldsymbol{\phi}}_z(k_0) = \boldsymbol{\phi}_z(k_0)/Q_\infty$. Furthermore, the steady solution is given by

$$
\begin{array}{rcl}
\bar{\boldsymbol{\mu}}_n(0) & = & -\left(\dfrac{\bar{U}_\infty}{\beta}\boldsymbol{n}_\xi + \bar{V}_\infty \boldsymbol{n}_\eta + \bar{W}_\infty \boldsymbol{n}_\zeta \right) \\[2mm]
\bar{\boldsymbol{\phi}}_x(0) & = & -\boldsymbol{K}_x(0)\bar{\boldsymbol{\mu}}_n(0), \ \ \bar{\boldsymbol{\phi}}_y(0) = -\boldsymbol{K}_y(0)\bar{\boldsymbol{\mu}}_n(0), \ \ \bar{\boldsymbol{\phi}}_z(0) = -\boldsymbol{K}_z(0)\bar{\boldsymbol{\mu}}_n(0)
\end{array}
$$

Consequently, the steady pressure distribution of equation 20 becomes

$$
\boldsymbol{c}_{p0} = 1 - \left(\bar{\boldsymbol{u}}(0) \circ \bar{\boldsymbol{u}}(0) + \bar{\boldsymbol{v}}(0) \circ \bar{\boldsymbol{v}}(0) + \bar{\boldsymbol{w}}(0) \circ \bar{\boldsymbol{w}}(0) \right) + M_\infty^2 \left(\bar{\boldsymbol{\phi}}_x(0) \circ \bar{\boldsymbol{\phi}}_x(0) \right)
\tag{28}
$$

Similarly, the oscillatory pressure distribution of equation 23 becomes

$$
\begin{array}{rcl}
\boldsymbol{c}_p(k_0) & = & -\dfrac{1}{\beta}(\bar{\boldsymbol{C}}_0 \circ \boldsymbol{n}_\xi)\bar{\boldsymbol{u}}_m - 2\bar{\boldsymbol{u}}(0) \circ \bar{\boldsymbol{u}}_m - (\bar{\boldsymbol{C}}_0 \circ \boldsymbol{n}_\eta)\bar{\boldsymbol{v}}_m - 2\bar{\boldsymbol{v}}(0) \circ \bar{\boldsymbol{v}}_m \\[2mm]
& & -(\bar{\boldsymbol{C}}_0 \circ \boldsymbol{n}_\zeta)\bar{\boldsymbol{w}}_m - 2\bar{\boldsymbol{w}}(0) \circ \bar{\boldsymbol{w}}_m + \dfrac{2\mathrm{i}k_0}{c_0\beta}(\bar{\boldsymbol{C}}_1 \circ \boldsymbol{n}_\xi)\bar{\boldsymbol{u}}_m \\[2mm]
& & +\dfrac{2\mathrm{i}k_0}{c_0}(\bar{\boldsymbol{C}}_1 \circ \boldsymbol{n}_\eta)\bar{\boldsymbol{v}}_m + \dfrac{2\mathrm{i}k_0}{c_0}(\bar{\boldsymbol{C}}_1 \circ \boldsymbol{n}_\zeta)\bar{\boldsymbol{w}}_m
\end{array}
\tag{29}
$$

where

$$
\begin{array}{rcl}
\bar{\boldsymbol{C}}_0(k_0) & = & 2M_\infty^2 \boldsymbol{K}_x(k_0) \circ \bar{\boldsymbol{\phi}}_x(0) - 2\boldsymbol{K}_x(k_0) \circ \bar{\boldsymbol{u}}(0) - 2\boldsymbol{K}_y(k_0) \circ \bar{\boldsymbol{v}}(0) \\[1mm]
& & -2\boldsymbol{K}_z(k_0) \circ \bar{\boldsymbol{w}}(0) \\[1mm]
\bar{\boldsymbol{C}}_1(k_0) & = & 2\boldsymbol{K}(k_0) - 2M_\infty^2 \boldsymbol{K}(k_0) \circ \bar{\boldsymbol{\phi}}_x(0)
\end{array}
$$

so that $\boldsymbol{c}_p(k_0)$ only depends on k_0 and M_∞.

Substituting from equations 26 into equation 29 yields

$$
\begin{array}{rcl}
\boldsymbol{c}_p(k_0) & = & \left(\boldsymbol{c}_{p_\phi}(k_0) + \boldsymbol{c}_{p_\theta}(k_0) + \boldsymbol{c}_{p_\psi}(k_0) \right) \boldsymbol{q}(k_0) \\[2mm]
& & +\mathrm{i}k_0 \left(\boldsymbol{c}_{p_{\dot{x}}}(k_0) + \boldsymbol{c}_{p_{\dot{y}}}(k_0) + \boldsymbol{c}_{p_{\dot{z}}}(k_0) + \boldsymbol{c}_{p_{\dot{\phi}}}(k_0) + \boldsymbol{c}_{p_{\dot{\theta}}}(k_0) + \boldsymbol{c}_{p_{\dot{\psi}}}(k_0) \right) \boldsymbol{q}(k_0) \\[2mm]
& & +(\mathrm{i}k_0)^2 \left(\boldsymbol{c}_{p_{\ddot{x}}}(k_0) + \boldsymbol{c}_{p_{\ddot{y}}}(k_0) + \boldsymbol{c}_{p_{\ddot{z}}}(k_0) \right) \boldsymbol{q}(k_0)
\end{array}
\tag{30}
$$

where the $N \times K$ matrices $\boldsymbol{c}_{p_\phi}(k_0)$, $\boldsymbol{c}_{p_\theta}(k_0)$, $\boldsymbol{c}_{p_{\dot{x}}}(k_0)$, $\boldsymbol{c}_{p_{\dot{y}}}(k_0)$, $\boldsymbol{c}_{p_{\ddot{x}}}(k_0)$, $\boldsymbol{c}_{p_{\ddot{y}}}(k_0)$, etc, can be referred to as pressure derivatives and are given by

$$
\boldsymbol{c}_{p_\phi}(k_0) = -\bar{W}_\infty \bar{C}_0(\tilde{\boldsymbol{\Phi}}_\phi \circ \boldsymbol{n}_\eta) - 2\bar{W}_\infty \bar{\boldsymbol{v}}(0) \circ \tilde{\boldsymbol{\Phi}}_\phi + \bar{V}_\infty \bar{C}_0(\tilde{\boldsymbol{\Phi}}_\phi \circ \boldsymbol{n}_\zeta) + 2\bar{V}_\infty \bar{\boldsymbol{w}}(0) \circ \tilde{\boldsymbol{\Phi}}_\phi
$$

$$
\boldsymbol{c}_{p_\theta}(k_0) = \frac{\bar{W}_\infty}{\beta} \bar{C}_0(\tilde{\boldsymbol{\Phi}}_\theta \circ \boldsymbol{n}_\xi) + 2\bar{W}_\infty \bar{\boldsymbol{u}}(0) \circ \tilde{\boldsymbol{\Phi}}_\theta - \bar{U}_\infty \bar{C}_0(\tilde{\boldsymbol{\Phi}}_\theta \circ \boldsymbol{n}_\zeta) - 2\bar{U}_\infty \bar{\boldsymbol{w}}(0) \circ \tilde{\boldsymbol{\Phi}}_\theta
$$

$$
\boldsymbol{c}_{p_\psi}(k_0) = -\frac{\bar{V}_\infty}{\beta} \bar{C}_0(\tilde{\boldsymbol{\Phi}}_\psi \circ \boldsymbol{n}_\xi) - 2\bar{V}_\infty \bar{\boldsymbol{u}}(0) \circ \tilde{\boldsymbol{\Phi}}_\psi + \bar{U}_\infty \bar{C}_0(\tilde{\boldsymbol{\Phi}}_\psi \circ \boldsymbol{n}_\eta) + 2\bar{U}_\infty \bar{\boldsymbol{v}}(0) \circ \tilde{\boldsymbol{\Phi}}_\psi
$$

$$
\boldsymbol{c}_{p_{\dot{x}}}(k_0) = -\frac{2}{c_0}\left(\frac{1}{\beta}\bar{C}_0(\tilde{\boldsymbol{\Phi}}_x \circ \boldsymbol{n}_\xi) + 2\bar{\boldsymbol{u}}(0) \circ \tilde{\boldsymbol{\Phi}}_x\right)
$$

$$
\boldsymbol{c}_{p_{\dot{y}}}(k_0) = -\frac{2}{c_0}\left(\bar{C}_0(\tilde{\boldsymbol{\Phi}}_y \circ \boldsymbol{n}_\eta) + 2\bar{\boldsymbol{v}}(0) \circ \tilde{\boldsymbol{\Phi}}_y\right)
$$

$$
\boldsymbol{c}_{p_{\dot{z}}}(k_0) = -\frac{2}{c_0}\left(\bar{C}_0(\tilde{\boldsymbol{\Phi}}_z \circ \boldsymbol{n}_\zeta) + 2\bar{\boldsymbol{w}}(0) \circ \tilde{\boldsymbol{\Phi}}_z\right)
$$

$$
\boldsymbol{c}_{p_{\dot{\phi}}}(k_0) = \frac{2}{c_0}\left(-\bar{W}_\infty \bar{C}_1(\tilde{\boldsymbol{\Phi}}_\phi \circ \boldsymbol{n}_\eta) + \bar{V}_\infty \bar{C}_1(\tilde{\boldsymbol{\Phi}}_\phi \circ \boldsymbol{n}_\zeta)\right)
$$

$$
\boldsymbol{c}_{p_{\dot{\theta}}}(k_0) = \frac{2}{c_0}\left(\frac{\bar{W}_\infty}{\beta}\bar{C}_1(\tilde{\boldsymbol{\Phi}}_\theta \circ \boldsymbol{n}_\xi) - \bar{U}_\infty \bar{C}_1(\tilde{\boldsymbol{\Phi}}_\theta \circ \boldsymbol{n}_\zeta)\right)
$$

$$
\boldsymbol{c}_{p_{\dot{\psi}}}(k_0) = \frac{2}{c_0}\left(-\frac{\bar{V}_\infty}{\beta}\bar{C}_1(\tilde{\boldsymbol{\Phi}}_\psi \circ \boldsymbol{n}_\xi) + \bar{U}_\infty \bar{C}_1(\tilde{\boldsymbol{\Phi}}_\psi \circ \boldsymbol{n}_\eta)\right)
$$

$$
\boldsymbol{c}_{p_{\ddot{x}}}(k_0) = -\frac{4}{\beta c_0^2}\bar{C}_1(\tilde{\boldsymbol{\Phi}}_x \circ \boldsymbol{n}_\xi)
$$

$$
\boldsymbol{c}_{p_{\ddot{y}}}(k_0) = -\frac{4}{c_0^2}\bar{C}_1(\tilde{\boldsymbol{\Phi}}_y \circ \boldsymbol{n}_\eta)
$$

$$
\boldsymbol{c}_{p_{\ddot{z}}}(k_0) = -\frac{4}{c_0^2}\bar{C}_1(\tilde{\boldsymbol{\Phi}}_z \circ \boldsymbol{n}_\zeta)
$$

The aerodynamic loads caused by the pressure distribution on each panel are given by

$$
\begin{aligned}
\boldsymbol{F}_x(k) &= \boldsymbol{c}_p(k) \circ \boldsymbol{s} \circ \boldsymbol{n}_x \\
\boldsymbol{F}_y(k) &= \boldsymbol{c}_p(k) \circ \boldsymbol{s} \circ \boldsymbol{n}_y \\
\boldsymbol{F}_z(k) &= \boldsymbol{c}_p(k) \circ \boldsymbol{s} \circ \boldsymbol{n}_z
\end{aligned}
\tag{31}
$$

where $\boldsymbol{F}_x(k)$, $\boldsymbol{F}_y(k)$, $\boldsymbol{F}_z(k)$, are $N \times K$ matrices of the aerodynamic loads per Pascal acting on each panel for each mode in the x, y and z directions and $\boldsymbol{s}$ the $N \times 1$ vector of the areas of the panels. Setting $k = 0$ and substituting for $\boldsymbol{c}_p(k_0)$ from equation 28 results in the steady aerodynamic loads

$$
\boldsymbol{F}_x(0) = \boldsymbol{c}_{p_0} \circ \boldsymbol{s} \circ \boldsymbol{n}_x, \ \ \boldsymbol{F}_y(0) = \boldsymbol{c}_{p_0} \circ \boldsymbol{s} \circ \boldsymbol{n}_y, \ \ \boldsymbol{F}_z(0) = \boldsymbol{c}_{p_0} \circ \boldsymbol{s} \circ \boldsymbol{n}_z
$$

Then, setting $k = k_0$ and substituting for $\boldsymbol{c}_p(k_0)$ from equation 30, the oscillatory aerodynamic loads can be written as

$$
\begin{aligned}
\boldsymbol{F}_x(k_0) &= \left(\boldsymbol{F}_{x_0}(k_0) + \mathrm{i}k_0\boldsymbol{F}_{x_1}(k_0) + (\mathrm{i}k_0)^2\boldsymbol{F}_{x_2}(k_0)\right)\boldsymbol{q}(k_0) \\
\boldsymbol{F}_y(k_0) &= \left(\boldsymbol{F}_{y_0}(k_0) + \mathrm{i}k_0\boldsymbol{F}_{y_1}(k_0) + (\mathrm{i}k_0)^2\boldsymbol{F}_{y_2}(k_0)\right)\boldsymbol{q}(k_0) \\
\boldsymbol{F}_z(k_0) &= \left(\boldsymbol{F}_{z_0}(k_0) + \mathrm{i}k_0\boldsymbol{F}_{z_1}(k_0) + (\mathrm{i}k_0)^2\boldsymbol{F}_{z_2}(k_0)\right)\boldsymbol{q}(k_0)
\end{aligned}
\tag{32}
$$

where

$$
\begin{aligned}
\boldsymbol{F}_{x_0}(k_0) &= \big(\boldsymbol{c}_{p_\phi}(k_0) + \boldsymbol{c}_{p_\theta}(k_0) + \boldsymbol{c}_{p_\psi}(k_0)\big) \circ \boldsymbol{s} \circ \boldsymbol{n}_x \\
\boldsymbol{F}_{x_1}(k_0) &= \big(\boldsymbol{c}_{p_{\dot{x}}}(k_0) + \boldsymbol{c}_{p_{\dot{y}}}(k_0) + \boldsymbol{c}_{p_{\dot{z}}}(k_0) + \boldsymbol{c}_{p_{\dot{\phi}}}(k_0) + \boldsymbol{c}_{p_{\dot{\theta}}}(k_0) + \boldsymbol{c}_{p_{\dot{\psi}}}(k_0)\big) \circ \boldsymbol{s} \circ \boldsymbol{n}_x \\
\boldsymbol{F}_{x_2}(k_0) &= \big(\boldsymbol{c}_{p_{\ddot{x}}}(k_0) + \boldsymbol{c}_{p_{\ddot{y}}}(k_0) + \boldsymbol{c}_{p_{\ddot{z}}}(k_0)\big) \circ \boldsymbol{s} \circ \boldsymbol{n}_x
\end{aligned}
$$

and similarly for the other two directions. The final step is to create aerodynamic load arrays that correspond to the degrees of freedom of the finite element model, i.e.

$$
\boldsymbol{F}(0) = \begin{pmatrix} F_{x_1}(0) \\ F_{y_1}(0) \\ F_{z_1}(0) \\ 0 \\ 0 \\ 0 \\ \vdots \\ F_{x_N}(0) \\ F_{y_N}(0) \\ F_{z_N}(0) \\ 0 \\ 0 \\ 0 \end{pmatrix}, \ \boldsymbol{F}(k_0) = \begin{pmatrix} F_{x_{1,1}}(k_0) & F_{x_{1,2}}(k_0) & \ldots & F_{x_{1,K}}(k_0) \\ F_{y_{1,1}}(k_0) & F_{y_{1,2}}(k_0) & \ldots & F_{y_{1,K}}(k_0) \\ F_{z_{1,1}}(k_0) & F_{z_{1,2}}(k_0) & \ldots & F_{z_{1,K}}(k_0) \\ 0 & 0 & \ldots & 0 \\ 0 & 0 & \ldots & 0 \\ 0 & 0 & \ldots & 0 \\ \vdots & \vdots & \ddots & \vdots \\ F_{x_{N,1}}(k_0) & F_{x_{N,2}}(k_0) & \ldots & F_{x_{N,K}}(k_0) \\ F_{y_{N,1}}(k_0) & F_{y_{N,2}}(k_0) & \ldots & F_{y_{N,K}}(k_0) \\ F_{z_{N,1}}(k_0) & F_{z_{N,2}}(k_0) & \ldots & F_{z_{N,K}}(k_0) \\ 0 & 0 & \ldots & 0 \\ 0 & 0 & \ldots & 0 \\ 0 & 0 & \ldots & 0 \end{pmatrix} \boldsymbol{q}(k_0)
$$

where $\boldsymbol{F}(0)$ is $6N \times 1$ vector, $\boldsymbol{F}(k_0)$ is a $6N \times K$ matrix, $F_{x_I}(0)$, $F_{y_I}(0)$, $F_{z_I}(0)$ are the elements of vectors $\boldsymbol{F}_x(0)$, $\boldsymbol{F}_y(0)$, $\boldsymbol{F}_z(0)$ and $F_{x_{I,J}}(k_0)$, $F_{y_{I,J}}(k_0)$, $F_{z_{I,J}}(k_0)$ the elements of matrices $\boldsymbol{F}_x(k_0)$, $\boldsymbol{F}_y(k_0)$, $\boldsymbol{F}_z(k_0)$ for $I = 1, \ldots, N$, $J = 1, \ldots, N$. The aeroelastic equation of motion becomes

$$
\boldsymbol{E}\mathbf{q}(0) = \frac{1}{2}\rho Q_\infty^2 \boldsymbol{Q}(0) \tag{33}
$$

for $k = 0$, where $\boldsymbol{Q}(0) = \tilde{\boldsymbol{\Phi}}^T \boldsymbol{F}(0)$, and

$$
\boldsymbol{A}\ddot{\mathbf{q}} + \boldsymbol{E}\mathbf{q} = \frac{1}{2}\rho Q_\infty^2 \boldsymbol{Q}(k_0)\mathbf{q} \tag{34}
$$

for $k = k_0$, where the $K \times K$ generalized aerodynamic force matrix is obtained from $\boldsymbol{Q}(k_0) = \tilde{\boldsymbol{\Phi}}^T \boldsymbol{F}(k_0)$. Alternatively, if the decomposition of equation 32 is used, equation 34 can be written as

$$
\boldsymbol{A}\ddot{\mathbf{q}} + \boldsymbol{E}\mathbf{q} = \frac{1}{2}\rho Q_\infty^2 \big(\boldsymbol{Q}_0(k_0) + \mathrm{i}k_0\boldsymbol{Q}_1(k_0) + (\mathrm{i}k_0)^2\boldsymbol{Q}_2(k_0)\big)\mathbf{q} \tag{35}
$$

where $\boldsymbol{Q}_0(k_0)$, $\boldsymbol{Q}_1(k_0)$, $\boldsymbol{Q}_2(k_0)$ are the $K \times K$ generalized aerodynamic stiffness, damping and mass matrices; $\boldsymbol{Q}_0(k_0)$ is calculated from the elements of matrices $\boldsymbol{F}_{x_0}(k_0)$, $\boldsymbol{F}_{y_0}(k_0)$, $\boldsymbol{F}_{z_0}(k_0)$, $\boldsymbol{Q}_1(k_0)$ from $\boldsymbol{F}_{x_1}(k_0)$, $\boldsymbol{F}_{y_1}(k_0)$, $\boldsymbol{F}_{z_1}(k_0)$ and $\boldsymbol{Q}_2(k_0)$ from $\boldsymbol{F}_{x_2}(k_0)$, $\boldsymbol{F}_{y_2}(k_0)$, $\boldsymbol{F}_{z_2}(k_0)$.

4 APPLICATION TO THE AGARD WING

The aeroelastic source and doublet panel method presented in this work is applied to the well-known weakened AGARD 445.6 wing experimental test case [11]. This flexible half-wing model had root chord of $c_0 = 0.589$ m, taper ratio $\lambda = 0.6576$, half-span $b/2 = 0.762$ m, sweep angle at the quarter-chord $\Lambda_{c/4} = 45°$, half aspect ratio 1.6525 and a NACA 65A004 airfoil section oriented in the streamwise direction. It was made of laminated mahogany but

was weakened by drilling holes in it and filling them with foam; its mass was 1.673 kg and the natural frequency of its first torsion mode $\omega_\alpha = 239.3$. It was installed at an angle of attack $\alpha_0 = 0°$ in the Langley Transonic Dynamics Tunnel and tested for flutter using both air and Freon as the testing medium. The free stream Mach numbers of the tests ranged from 0.34 to 1.14.

The finite element model for the weakened AGARD 445.6 wing was constructed using the Equivalent Plate Method (EPM) [12, 13]. Non-zero mode shapes were obtained for $\boldsymbol{\Phi}_z$, $\boldsymbol{\Phi}_\phi$ and $\boldsymbol{\Phi}_\theta$; displacements x and y were negligible and the model does not have a degree of freedom in the ψ direction. Figure 1 plots the first four mode shapes in the z direction, $\boldsymbol{\Phi}_z$, obtained using the model. The first mode features mainly bending, mdoe 2 mainly torsion, mode 3 combines both bending and torsion while mode features mainly torsion. Table 1 compares the natural frequencies of the five modes obtained from the EPM to the experimentally measured data. Structural damping was not measured during the experiments but the damping ratio was estimated to be $\zeta = 0.02$ [11]. Consequently, a structural damping matrix was created using

$$\boldsymbol{C} = \mathrm{diag}(2\zeta\boldsymbol{\omega}_n)$$

where $\boldsymbol{\omega}_n$ is the $K \times 1$ vector whose elements are the natural frequencies calculated from the finite element model, noting that matrix $\boldsymbol{A}$ is the unit matrix and $\boldsymbol{E}$ features the squares of the natural frequencies on its diagonal.

Table 1: Natural frequencies in Hz of the first five mode shapes of the weakened AGARD 445.6 wing

	Mode 1	Mode 2	Mode 3	Mode 4	Mode 5
FE model	9.67	40.07	50.30	96.55	125.58
Experiment	9.60	38.17	48.35	91.54	118.11

The flat mode shapes calculated by the finite element model were applied to both the upper and lower surfaces of the SDPM model. The mode shapes were interpolated onto the control points for the SDPM panels and mirrored across the $y = 0$ plane in order to represent the complete wing geometry. Then, the same modal displacements were applied to both the upper surface and the lower surface. Nevertheless, as the structural matrices represent the dynamics of a half-wing, the generalized aerodynamic matrices of equations 33 to 35 were calculated from $\boldsymbol{Q}(0) = \tilde{\boldsymbol{\Phi}}^T \boldsymbol{F}(0)/2$, $\boldsymbol{Q}(k_0) = \tilde{\boldsymbol{\Phi}}^T \boldsymbol{F}(k_0)/2$ and similarly for $\boldsymbol{Q}_0(k_0)$, $\boldsymbol{Q}_1(k_0)$, $\boldsymbol{Q}_2(k_0)$.

The SDPM grid spacing was chosen to be nonlinear in both the chordwise and spanwise directions, such that the grid was finest around the leading edge and wingtips. A grid convergence study was carried out to choose the optimal values for m and n, the chordwise and spanwise numbers of panels. In all cases, the number of chordwise wake panels was set to $m_w = 10m$, such that the grid extended to 10 root chords downstream of the trailing edge. The flutter cases simulated concerned the tests carried out in air at Mach numbers ranging from 0.499 to 0.96.

As the aeroelastic system contains structural damping, equation 35 was modified to

$$\boldsymbol{A}\ddot{\mathbf{q}} + \boldsymbol{C}\dot{\mathbf{q}} + \boldsymbol{E}\mathbf{q} = \frac{1}{2}\rho Q_\infty^2 \left(\boldsymbol{Q}_0(k) + \mathrm{i}k\boldsymbol{Q}_1(k) + (\mathrm{i}k)^2\boldsymbol{Q}_2(k)\right)\mathbf{q} \tag{36}$$

and was solved using determinant iteration. First, matrices $\boldsymbol{Q}_0(k_j)$, $\boldsymbol{Q}_1(k_j)$ and $\boldsymbol{Q}_2(k_j)$ were calculated at 10 reduced frequency values, k_j, between 0.001 and 2.0. Then, the determinant

(a) Mode 1

(b) Mode 2
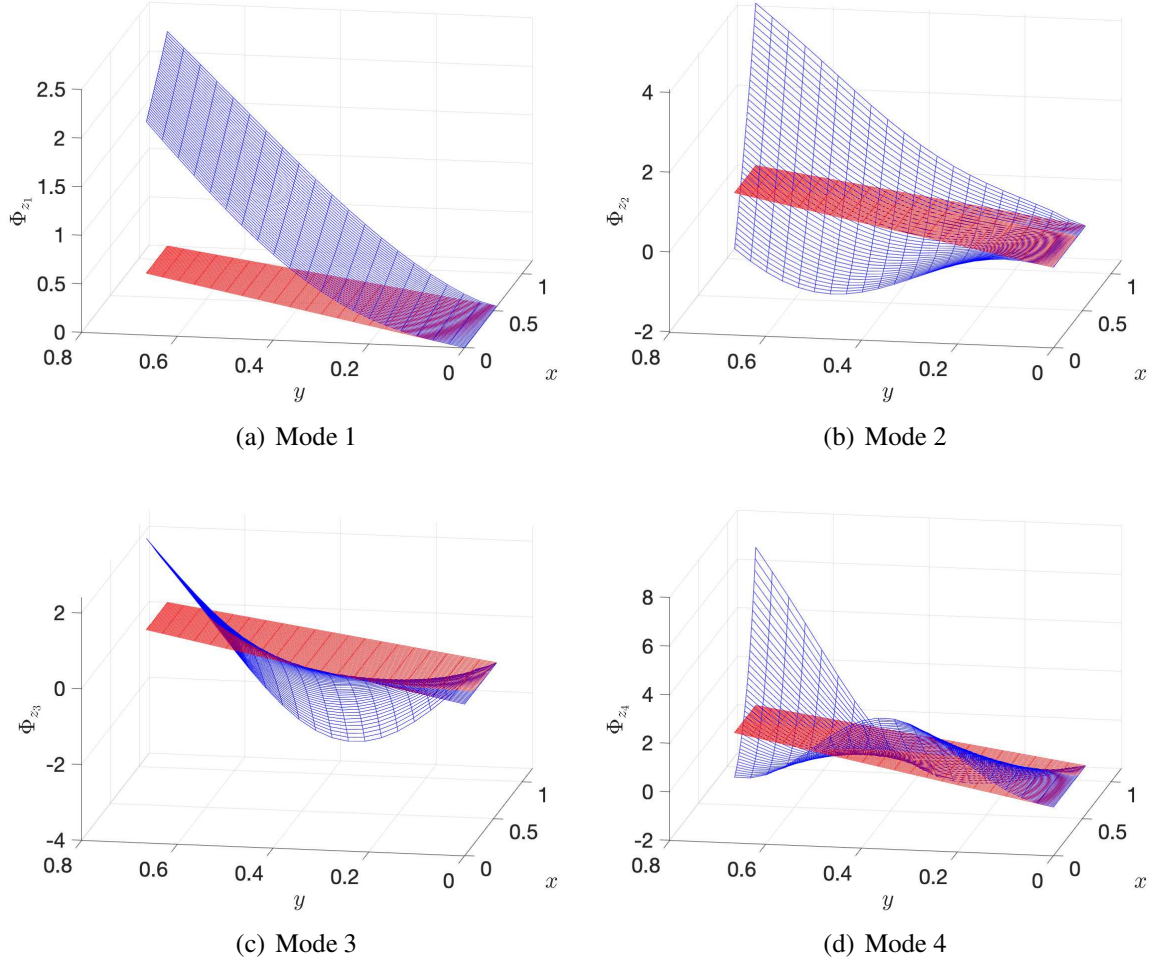

(c) Mode 3

(d) Mode 4

Figure 1: First four out-of-plane mode shapes, $\mathbf{\Phi}_z$, calculated for the weakened AGARD 445.6 wing using the Equivalent Plate Method

problem

$$
\begin{aligned}
D \;=\; & \left| \left(\frac{4Q_\infty^2}{c_0^2}\boldsymbol{A} - \frac{1}{2}\rho Q_\infty^2 \boldsymbol{Q}_2(k) \right) p^2 + \left(\frac{2Q_\infty}{c_0}\boldsymbol{C} - \frac{1}{2}\rho Q_\infty^2 \boldsymbol{Q}_1(k) \right) p \right. \\
& \left. + \left(\boldsymbol{E} - \frac{1}{2}\rho Q_\infty^2 \boldsymbol{Q}_0(k) \right) \right| = 0
\end{aligned}
$$

was solved using a Newton-Raphson procedure, where $p = g + \mathrm{i}k$ is one of the system's eigenvalues at airspeed Q_∞. There are two equations $\Re(D) = 0$, $\Im(D) = 0$, with two unknowns, g and k. The experimental results give the free stream Mach number, airspeed, speed of sound and density of the flutter points identified. Two options exist for the calculation:

- Set the free stream density to the experimentally measured value and carry out determinant iterations in order to calculate the flutter airspeed and frequency.
- As the flutter point is matched and the free stream Mach number and speed of sound are known, the flutter speed can be considered to be known. Then, determinant iterations can be carried out to calculate the flutter density and frequency.

The two approaches give identical results for the flutter frequency and flutter speed index, de-

fined as

$$Q_F^* = \frac{2Q_F}{c_0 \omega_\alpha \sqrt{\mu}} \tag{37}$$

where Q_F is the flutter airspeed in m/s and μ is the mass ratio. The first approach ensures that the free stream density is identical to the one measured experimentally, while the second ensures that the flutter point is matched.

(a) Q_F^* (b) ω_F/ω_{alpha}
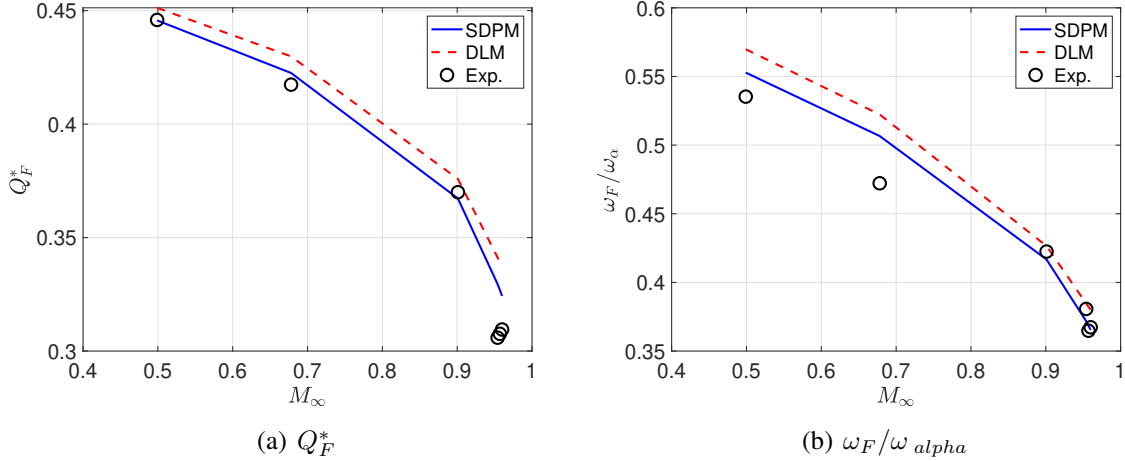
Figure 2: Flutter predictions by the SDPM and DLM for the AGARD wing

The AGARD wing flutter problem was also solved using the Doublet Lattice method for comparison purposes. The generalized aerodynamic force matrix was calculated by means of a re-implementation of the DLM technique by Blair [5, 14] and the flutter points were obtained using the modified p-k method [15, 16]; the finite element modes were those used for the SDPM calculations. Figure 2 plots the flutter airspeeds and frequencies obtained from the SDPM and DLM for all the subsonic Mach number test cases and compares them to the experimental measurements. The wind-off natural frequency of the second mode predicted by the finite element model was used for ω_α. It should be stressed that both the SDPM and DLM cannot predict shock waves so that their predictions for $M_\infty > 0.7$ are not reliable. Nevertheless, it can be seen that both sets of predictions follow closely the experimental data up to $M_\infty = 0.9$, noting that the SDPM results are in slightly better agreement with the wind tunnel measurements.

5 APPLICATION TO THE NASA BENCHMARK RECTANGULAR WINGS

NASA tested three rectangular finite wing models with pitch and plunge degrees of freedom at the Langley Transonic Dynamics Tunnel [17–19]. The half-wing models had the same dimensions and aspect ratios but different cross sections. The span was $b = 1.63$ m (half-span 0.81 m) and the constant chord $c_0 = 0.41$ m, resulting in a half-wing aspect ratio of 2 (full aspect ratio of 4). The three chosen cross sections were NACA 0012, NACA 64A010 and NASA SC(2) 0414. The wings were rigid but were suspended from a flexible structure known as the Pitch and Plunge Apparatus (PAPA) [20], giving them plunge, h, and pitch around the half-chord, α, degrees of freedom. The structural mass and stiffness matrices are given by

$$\boldsymbol{A} = \begin{pmatrix} m & 0 \\ 0 & I_\alpha \end{pmatrix}, \ \boldsymbol{E} = \begin{pmatrix} K_h & 0 \\ 0 & K_\alpha \end{pmatrix}$$

where m is the mass of the wing, I_α its moment of inertia around the pitch axis, $x_f = c_0/2$ the chordwise position of the pitch axis, K_h the stiffness of the suspension mechanism in the

plunge direction and K_α the stiffness in the pitch direction. Only one set of structural parameters is given in [19] for the three wings, stating that this set is representative of all three systems. However, slightly different parameter values are given in [17] for the NACA 0012 and in [18] for the NASA SC(2) 0414, wich is also referred to as the Benchmark SuperCritical Wing (BSCW). The three sets of values are given here in table 2, where ω_h and ω_α are the uncoupled, wind-off natural frequencies in plunge and pitch respectively.

Table 2: Structural parameters of the three benchmark models

Wing	m (kg)	I_α (kg.m^2)	K_h (N/m)	K_α (Nm/rad)	ω_h (rad/s)	ω_α (rad/s)
NACA 0012	87.07	3.68	3.88×10^4	3.93×10^3	21.11	32.67
NACA 64A010	87.91	3.76	3.84×10^4	4.01×10^3	20.92	32.67
NASA SC(2) 0414	88.44	3.69	3.85×10^4	4.02×10^3	20.86	32.99

The structural damping is given as 0.0024 or 0.001 for both degrees of freedom, depending on the reference, but it is unclear if this value was a decay rate or the damping ratio. As the structural damping of the PAPA system is very low [20], structural damping was ignored in the present work. The wings were tested at a range of Mach numbers between 0.3 and 0.95 in both air and R-12 heavy gas.

In this case, the body is rigid body and the relative velocity between the flow and the wing is defined by the plunge displacement, $h(t)$, defined positive downwards, and the pitch rotation $\alpha(t)$ around the pitch axis, $\mathbf{x}_f = (x_f,\ y_f,\ z_f)$, defined positive nose-up. Then,

$$
\begin{aligned}
\boldsymbol{u}_{\mathrm{rel}}(t) &= -\dot{\alpha}(t)(\boldsymbol{z}_c - z_f) \\
\boldsymbol{v}_{\mathrm{rel}}(t) &= \mathbf{0} \\
\boldsymbol{w}_{\mathrm{rel}}(t) &= Q_\infty \alpha(t) + \dot{\alpha}(t)(\boldsymbol{x}_c - x_f) + \dot{h}(t)
\end{aligned}
\tag{38}
$$

where $\boldsymbol{x}_c,\ \boldsymbol{y}_c,\ \boldsymbol{z}_c$ are the $N \times 1$ vectors whose elements are the x, y and z coordinates of the control points. Note that h is defined positive downwards in equations 38, which is the standard Theodorsen theory definition. The SDPM solution procedure is similar to the one developed for flexible motion but the pressure derivatives are simplified to

$$
\begin{aligned}
\boldsymbol{c}_{p_{\dot{h}}}(k_0) &= -\frac{2}{c_0}\left(\bar{\boldsymbol{C}}_0 \boldsymbol{n}_\zeta + 2\bar{\boldsymbol{w}}(0)\right) \\[2mm]
\boldsymbol{c}_{p_{\ddot{h}}}(k_0) &= -\left(\frac{2}{c_0}\right)^2 \bar{\boldsymbol{C}}_1 \boldsymbol{n}_\zeta \\[2mm]
\boldsymbol{c}_{p_\alpha}(k_0) &= -\bar{U}_\infty \left(\bar{\boldsymbol{C}}_0 \boldsymbol{n}_\zeta + 2\bar{\boldsymbol{w}}(0)\right) \\[2mm]
\boldsymbol{c}_{p_{\dot{\alpha}}}(k_0) &= \frac{2}{c_0}\left(\frac{1}{\beta}\bar{\boldsymbol{C}}_0 \left(\boldsymbol{n}_\xi \circ (\boldsymbol{\zeta}_c - \zeta_f)\right) - \bar{\boldsymbol{C}}_0 \left(\boldsymbol{n}_\zeta \circ (\boldsymbol{\xi}_c - \xi_f)\right) - \bar{U}_\infty \bar{\boldsymbol{C}}_1 \boldsymbol{n}_\zeta\right. \\[2mm]
&\quad \left. + 2\bar{\boldsymbol{u}}(0) \circ (\boldsymbol{\zeta}_c - \zeta_f) - 2\bar{\boldsymbol{w}}(0) \circ (\boldsymbol{\xi}_c - \xi_f)\right) \\[2mm]
\boldsymbol{c}_{p_{\ddot{\alpha}}}(k_0) &= \left(\frac{2}{c_0}\right)^2 \left(\frac{1}{\beta}\bar{\boldsymbol{C}}_1 \left(\boldsymbol{n}_\xi \circ (\boldsymbol{\zeta}_c - \zeta_f)\right) - \bar{\boldsymbol{C}}_1 \left(\boldsymbol{n}_\zeta \circ (\boldsymbol{\xi}_c - \xi_f)\right)\right)
\end{aligned}
\tag{39}
$$

such that the complete oscillatory pressure is given by

$$
\begin{aligned}
\boldsymbol{c}_p(k_0) &= \boldsymbol{c}_{p_\alpha}(k_0)\alpha(k_0) + \mathrm{i}k_0\left(\boldsymbol{c}_{p_{\dot{h}}}(k_0)h(k_0) + \boldsymbol{c}_{p_{\dot{\alpha}}}(k_0)\alpha(k_0)\right) \\
&\quad + (\mathrm{i}k_0)^2 \left(\boldsymbol{c}_{p_{\ddot{h}}}(k_0)h(k_0) + \boldsymbol{c}_{p_{\ddot{\alpha}}}(k_0)\alpha(k_0)\right)
\end{aligned}
\tag{40}
$$

14

The aerodynamic load and moment derivatives around the pitch axis are given by

$$
\begin{aligned}
\boldsymbol{F}_{x_\alpha}(k_0) &= -\boldsymbol{c}_{p_\alpha}(k_0) \circ \boldsymbol{s} \circ \boldsymbol{n}_x \\
\boldsymbol{F}_{y_\alpha}(k_0) &= -\boldsymbol{c}_{p_\alpha}(k_0) \circ \boldsymbol{s} \circ \boldsymbol{n}_y \\
\boldsymbol{F}_{z_\alpha}(k_0) &= -\boldsymbol{c}_{p_\alpha}(k_0) \circ \boldsymbol{s} \circ \boldsymbol{n}_z \\
\boldsymbol{M}_{x_\alpha}(k_0) &= -\boldsymbol{c}_{p_\alpha}(k_0) \circ \boldsymbol{s} \circ (-\boldsymbol{n}_y \circ (\boldsymbol{z}_c - z_f) + \boldsymbol{n}_z \circ (\boldsymbol{y}_c - y_f)) \\
\boldsymbol{M}_{y_\alpha}(k_0) &= -\boldsymbol{c}_{p_\alpha}(k_0) \circ \boldsymbol{s} \circ (\boldsymbol{n}_x \circ (\boldsymbol{z}_c - z_f) - \boldsymbol{n}_z \circ (\boldsymbol{x}_c - x_f)) \\
\boldsymbol{M}_{z_\alpha}(k_0) &= -\boldsymbol{c}_{p_\alpha}(k_0) \circ \boldsymbol{s} \circ (-\boldsymbol{n}_x \circ (\boldsymbol{y}_c - y_f) + \boldsymbol{n}_y \circ (\boldsymbol{x}_c - x_f))
\end{aligned}
$$

and similarly for the derivatives with respect to $\dot{h}, \dot{\alpha}, \ddot{h}, \ddot{\alpha}$. The aerodynamic stiffness, damping and mass matrices are given by

$$
\boldsymbol{Q}_0(k_0) = \begin{pmatrix} 0 & -\sum_{i=1}^N \boldsymbol{F}_{z_\alpha}(k_0) \\ 0 & \sum_{i=1}^N \boldsymbol{M}_{y_\alpha}(k_0) \end{pmatrix}, \ \boldsymbol{Q}_1(k_0) = \begin{pmatrix} -\sum_{i=1}^N \boldsymbol{F}_{z_{\dot{h}}}(k_0) & -\sum_{i=1}^N \boldsymbol{F}_{z_{\dot{\alpha}}}(k_0) \\ \sum_{i=1}^N \boldsymbol{M}_{y_{\dot{h}}}(k_0) & \sum_{i=1}^N \boldsymbol{M}_{y_{\dot{\alpha}}}(k_0) \end{pmatrix}
$$

$$
\boldsymbol{Q}_2(k_0) = \begin{pmatrix} -\sum_{i=1}^N \boldsymbol{F}_{z_{\ddot{h}}}(k_0) & -\sum_{i=1}^N \boldsymbol{F}_{z_{\ddot{\alpha}}}(k_0) \\ \sum_{i=1}^N \boldsymbol{M}_{y_{\ddot{h}}}(k_0) & \sum_{i=1}^N \boldsymbol{M}_{y_{\ddot{\alpha}}}(k_0) \end{pmatrix}
$$

where all derivatives of $\boldsymbol{F}_z$ are negative because $\boldsymbol{F}_z$ is defined as positive downwards in Theodorsen theory. The aeroelastic equation of motion of expression 36 is then set up and solved using the determinant iteration technique, noting that $\mathbf{q} = (h \ \alpha)^T$.

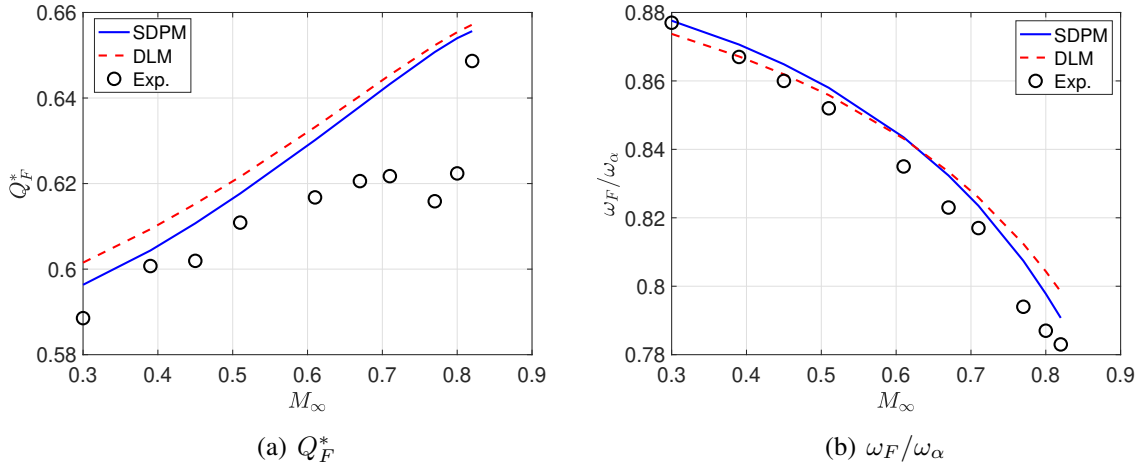

(a) Q_F^*

(b) ω_F/ω_α

Figure 3: Flutter predictions by the SDPM and DLM for the rectangular NACA 0012 wing

Figure 3 plots the flutter speed index and frequency ratio predicted by the SDPM and DLM for the rectangular NACA 0012 wing and compares them to the experimental measurements. Note that there is a question mark on the experimental calculation of the flutter speed index; the frequency used does not appear to be the wind-off uncoupled pitch natural frequency but 34.2 rad/s, a frequency that is not mentioned anywhere in [17] or [19]. As a consequence, the experimental values of the flutter speed index plotted in figure 3(a) were re-calculated using the standard definition of equation 37 and the value of ω_α given in table 2 for the NACA 0012 wing. Figure 3(a) shows that the flutter dip for this system occurs very early, at around $M_\infty = 0.77$. The NACA 0012 is a thick airfoil and shock waves occur on its surface at relatively low Mach numbers. The SDPM predictions for Q_F^* follow closely the experimental data up to $M_\infty = 0.51$ but the method fails to predict the flutter dip, since if cannot model shock waves. The DLM estimates for the flutter speed index are slightly overestimated compared to both the SDPM

results and the experimental measurements. The flutter frequency ratios predicted by both panel methods are in good agreement with experimental measurements, with maximum errors of around 2%.
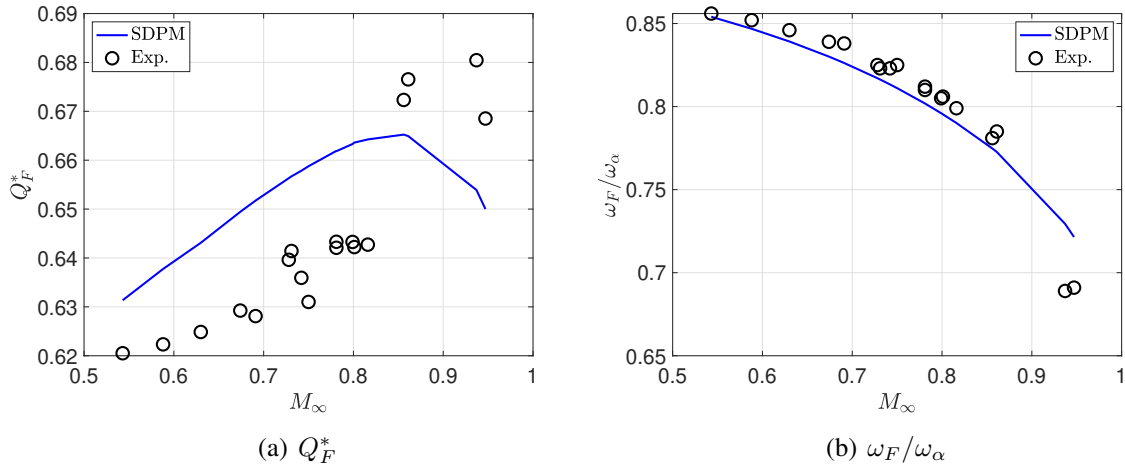

Figure 4: Flutter predictions by the SDPM for the rectangular NACA 64A010 wing

Figure 4(a) plots the flutter speed index and frequency ratio predicted by the SDPM for the rectangular NACA 0012 wing and compares them to the experimental measurements. The mean pitch angle was set to $\alpha_0 = 0.40° - 0.48°$, except for the flutter points at $M_\infty > 0.9$, for which $\alpha_0 = 0°$. Equations 39 show that the value of α_0 is taken into account by the SDPM through the values of $\bar{\boldsymbol{u}}(0)$ and $\bar{\boldsymbol{w}}(0)$. It can be seen that the flutter speed index calculated by the SDPM is overestimated for $M_\infty \leq 0.81$ and underestimated for $M_\infty > 0.81$. Nevertheless, the maximum error in Q_F^* is around 4.4%. The experimental data show that the flutter dip probably occurs at around $M_\infty = 0.75$. The SDPM frequency ratio predictions are very accurate up the flutter points occurring at $M_\infty > 0.9$, $\alpha_0 = 0°$. These points are characterized as 'plunge flutter' in [19] and have significantly lower frequency than the SDPM prediction. Nevertheless, the SDPM is not expected to represent accurately any of the flutter points occurring at or beyond the flutter dip.
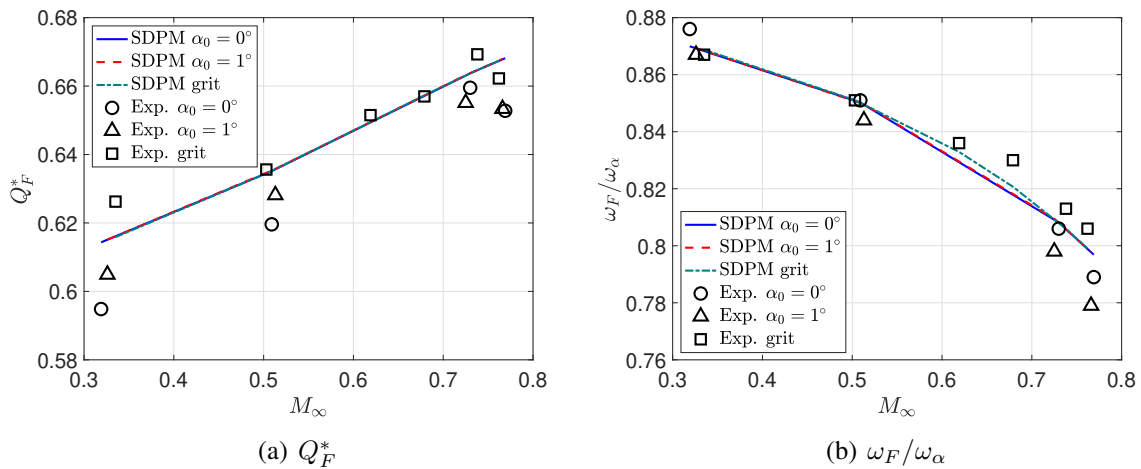

Figure 5: Flutter predictions by the SDPM for the rectangular NASA SC(2) 0414 wing (BSCW)

Figure 4(a) plots the flutter speed index and frequency ratio predicted by the SDPM for the rectangular NASA SC(2) 0414 wing and compares them to the experimental measurements.

16

Here, the results denoted by $\alpha_0 = 0°$ and $\alpha_0 = 1°$ were obtained with free transition while those denoted by grit were obtained iwith $\alpha_0 = 0°$ and fixed transition. The SDPM is an inviscid technique so that the transition position cannot affect its predictions. Only Mach number and mean angle of attack effects can be represented by the method. Nevertheless, it can be seen that the SDPM predicts flutter indices and frequency ratios closer to the fixed transition experimental measurements and that the change in α_0 from $0°$ to $1°$ has a very small effect on its predictions. The experiments show a higher sensitivity to the value of α_0, albeit for the free transition case.

6 CONCLUSIONS

This work has presented a development of the unsteady compressible source and double panel method in order to predict subsonic flutter. The main advantages of this approach with respect to the traditional Doublet Panel Method are:

- The complete pressure distribution around the exact surface is calculated.
- The pressure is calculated from a nonlinear second order version of Bernoulli's equation.
- The oscillatory pressure is written in terms of the derivatives of the pressure with respect to the modes, such that aerodynamic stiffness, damping and mass contributions can be evaluated separately.
- The surface motion is not limited to the out-of-plane direction; mode shapes can have components in all six degrees of freedom.
- The flutter predictions of the SDPM lie closer to the experimental validation data than those of the DLM.

As a final thought, it should be stated that a transonic correction technique has also been developed for the SDPM in order to correct its unsteady pressure predictions using steady pressure distributions calculated by a higher fidelity method [21]. This technique has already been extended to flutter solutions [22].

7 REFERENCES

[1] Morino, L., Chen, L., and Suciu, E. O. (1975). Steady and oscillatory subsonic and supersonic aerodynamics around complex configurations. *AIAA Journal*, 13(3), 368–374. doi:https://doi.org/10.2514/3.49706.

[2] Morino, L. and Chen, L.-T. (1975). Indicial compressible potential aerodynamics around complex aircraft configurations. In *Aerodynamic Analyses Requiring Advanced Computers Conference, NASA SP-347*. Hampton, VA, pp. 1067–1110.

[3] Morino, L. (1980). Steady, oscillatory and unsteady subsonic and supersonic aerodynamic forces - production version (SOUSSA-P 1.1) - volume I - theoretical manual. Contractor Report CR-159130, NASA.

[4] Martínez, M. S. and Dimitriadis, G. (2022). Subsonic source and doublet panel methods. *Journal of Fluids and Structures*, 113, 103624. doi:https://doi.org/10.1016/j.jfluidstructs.2022.103624.

[5] Dimitriadis, G. (2023). *Unsteady Aerodynamics - Potential and Vortex Methods*. Wiley. doi:https://doi.org/10.1002/9781119762560.

[6] Dimitriadis, G., Panagiotou, P., Dimopoulos, T., et al. (2024). Prediction of aerodynamic loads and stability derivatives using the unsteady source and doublet panel method for bwb configurations. In *Proceedings of the AIAA Scitech 2024 Forum*. Orlando, FL.

[7] Dimitriadis, G., Panagiotou, P., Dimopoulos, T., et al. (2024). Aerodynamic stability derivative calculations using the compressible source and doublet panel method. *Journal of Aircraft*, In print.

[8] Epton, M. A. and Magnus, A. E. (1990). PAN AIR- a computer program for predicting subsonic or supersonic linear potential flows about arbitrary configurations using a higher order panel method. Contractor Report CR-3251, NASA.

[9] Morino, L. (1974). A general theory of unsteady compressible potential aerodynamics. Contractor Report CR-2464, NASA.

[10] Hess, J. L. and Smith, A. M. O. (1967). Calculation of potential flow about arbitrary bodies. *Progress in Aerospace Sciences*, 8(1), 1–138. doi:https://doi.org/10.1016/0376-0421(67)90003-6.

[11] Carson Yates, Jr, E. (1988). AGARD standard aeroelastic configurations for dynamic response I – wing 445.6. Report AGARD-R-765, AGARD.

[12] Kafkas, A., Kilimtzidis, S., Kotzakolios, A., et al. (2021). Multi-fidelity optimization of a composite airliner wing subject to structural and aeroelastic constraints. *Aerospace*, 8, 398. doi:https://doi.org/10.3390/aerospace8120398.

[13] Kilimtzidis, S., Kotzakolios, A., and Kostopoulos, V. (2023). Efficient structural optimisation of composite materials aircraft wing. *Composite Structures*, 303, 116268. doi:10.1016/j.compstruct.2022.116268.

[14] Blair, M. (1994). A compilation of the mathematics leading to the doublet-lattice method. Report WL-TR-95-3022, Air Force Wright Laboratory.

[15] Rodden, W. P. (1987). *Handbook for Aeroelastic Analysis*, vol. 1. MSC/NASTRAN Ver. 65.

[16] Chen, P. C. (2000). Damping perturbation method for flutter solution: The g-method. *AIAA Journal*, 38(9), 1519–1524. doi:https://doi.org/10.2514/2.1171.

[17] Rivera, Jr, J. A., Dansberry, B. E., Durham, M. H., et al. (1992). Pressure measurements on a rectangular wing with a naca0012 airfoil during conventional flutter. Technical Memorandum TM-104211, NASA.

[18] Dansberry, B. E., Durham, M. H., Bennett, R. M., et al. (1993). Experimental unsteady pressures at flutter on the supercritical wing benchmark model. In *34th AIAA Structures, Structural Dynamics, and Materials Conference*. La Jolla, CA.

[19] Bennett, R. M. (2000). Test cases for flutter of the benchmark models rectangular wings on the pitch and plunge apparatus. In Various (Ed.), *Compendium of unsteady aerodynamic measurements*, AGARD-TR-26. AGARD, pp. 173–200.

[20] Farmer, M. G. (1982). A two-degree-of-freedom flutter mount system with low damping for testing rigid wings at different angles of attack. Technical Memorandum TM-83302, NASA.

[21] Crovato, A., Kilimtzidis, S., Sánchez Martínez, M., et al. (2024). Transonic corrections for the unsteady compressible source and doublet panel method. In *Proceedings of the AIAA Scitech 2024 Forum*. Orlando, FL.

[22] Dimitriadis, G., Crovato, A., Sanchez Martinez, M., et al. (2024). Transonic corrections for the unsteady compressible source and doublet panel method. *Journal of Aircraft*, Under review.

COPYRIGHT STATEMENT